Experimental study of slender LCFST columns connected by steel linking plates

Experimental study of slender LCFST columns connected by steel linking plates

Minyang Xu[1],Ting Zhou[1,3*],Zhihua Chen[1,2],, Yanbo Li[1], Luke Bisby[4]

1 Tianjin University, Tianjin, China

2 Tianjin Key Laboratory of Civil Engineering Structure and New Materials, Tianjin University, Tianjin, China

3 Tianjin Key Laboratory of Architectural Physics and Environmental Technology, Tianjin University, Tianjin, China

4 School of Engineering, University of Edinburgh, Edinburgh, EH93JN, UK

Abstract: This paper presents the results of an experimental investigation of L-shaped columns composed of concrete-filled steel tubes (LCFST columns) connected by steel linking plates. As a new kind of composite column, the fundamental structural behavior of LCFST columns connected by steel linking plates is discussed in this paper. Eight large-scale LCFST columns were constructed and loaded under either concentric axial compression or biaxial eccentric compression up to failure. Slenderness ratio, thickness of the steel linking plates and load eccentricities were all studied within the experimental programme. The relationships of load versus longitudinal displacement, lateral deflection at mid-height, longitudinal strain at mid-height etc are presented. It is demonstrated that specimens with larger slenderness ratios or eccentricities have lower ultimate load capacities, as expected. It is also demonstrated that the steel connection plates, also as expected, have a considerable influence on confining lateral deflections of the mono CFST columns

---

* Corresponding author: Ting Zhou. Telephone number:+8615822886836. Email: tdjgtingzhou@163.com

and that they significantly contribute to the columns' ultimate carrying capacity. Predictive formulas for calculating the ultimate loads of LCFST columns connected by steel linking plates are proposed based on modifications of the ANSI/AISC 360-05 guidelines.

Keywords: L-shaped composite columns; Experimental investigation; Concrete-filled steel tubes; Steel linking plates; Axial compression; Eccentric compression

1 Introduction

In recent years, various types of novel columns for applications in buildings have been widely used and studied all around the world. L-shaped reinforced concrete columns were first studied and the basic structural behavior of this kind of column under concentric or eccentric axial compressive loading was previously investigated by [1-3]. With the advent of high strength concrete and steel, these materials have also been used in L-shaped reinforced concrete columns. Tokgoz et al.[4] experimentally studied the behavior of L-shaped section steel fiber reinforced high strength reinforced concrete and steel-concrete composite columns under eccentric axial compression. Recently, with the increasing usage and popularity of concrete-filled steel tubular columns, owing to their highly efficient load carrying capabilities, inherent deformability and excellent energy dissipation properties, concrete-filled L-shaped (and other novel shaped) steel tube columns have been proposed and studied in considerable detail. For example, Yang et al.[5] studied the compressive behavior of T-shaped concrete-filled steel tubular columns. The seismic behavior of concrete-filled unconventional-shaped steel tube columns was also experimentally investigated by [6] , demonstrating that all the specimens exhibited favorable energy dissipation and ductility. Due to the weak bond between the special-shaped steel tubes and concrete in-fill, relative slippage between the two materials was observed to occur

at failure.

To improve the properties of concrete-filled novel-shaped steel tube columns, various shapes of columns composed of concrete-filled steel tubes (SCFST columns) linked by shear connections were proposed by Chen et al. [7,8]. Three cross-sectional shapes of L-shape, T-shape, as well as crisscross-shaped columns, when used as corner columns, side columns, and middle columns were previously proposed and experimentally studied. Because of the small width of the concrete filled steel tube mono columns in SCFST columns, SCFST columns can be embedded within the walls of buildings, which in turn enlarges the usable area of the buildings, with obvious benefits for developers. The fundamental structural behavior of SCFST columns connected by 'lacing bars' (i.e. effectively trussed CFST columns) under axial compression was studied by [9].

Based on the research above, SCFST columns connected by steel linking plates were proposed as shown in Fig.1. Two LCFST columns connected by steel linking plates were tested to investigate the effect of inner concrete on the behavior of the columns by Zhou et al. [10]. The behavior of the columns subjected to constant axial load and cyclically varying flexural load was also investigated by Zhou et al. [11]. Furthermore, related research on the heat transfer properties of this new kind of LCFST column, with a view to better understanding their fire resistance have been carried out using finite element methods [12].The seismic performance of frame structures composed of this novel kind of LCFST columns was also recently experimentally studied [13]. Nonetheless, research on this type of LCFST column is limited to date, and a large number of relevant parameters have yet to be investigated.

In the current study, eight large-scale L-shaped specimens were tested under either axial compression or biaxial eccentric compression. Parameters studied include

slenderness ratio, thickness of steel linking plates and the eccentricities of applied axial compressive load were selected to analyze their effects on the failure modes and deformation processes of LCFST columns. Specimen layout and experimental setup are described first, followed by discussion of the effects of the three aforementioned parameters on the response of the columns under compressive loading, including load-longitudinal displacement relationships, load-lateral deflection relationships and load-longitudinal strain relationships are presented. LCFST columns connected by steel linking plates are then compared against LCFST columns connected by so-called 'lacing bars' to clearly demonstrate their advantages. Finally, the experimental results are compared with predicted values obtained from proposed formulae based on modification of the ANSI/AISC 360-05[14] guidelines.

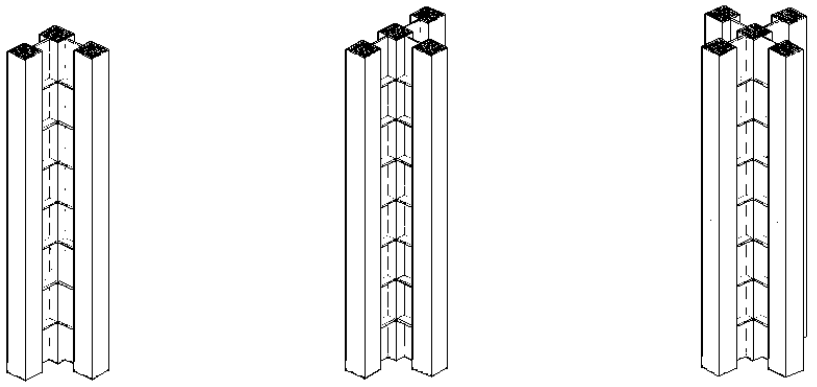

(a) L-shape **(b) T-shape** **(c) Crisscross-shape**

Fig.1 SCFST columns connected by steel linking plates

2 Experimental program

2.1 Introduction

Eight large-scale LCFST columns were fabricated and tested. The primary objective of the testing was to study the effects of various parameters including: slenderness ratio, thickness of the steel linking plates and the eccentricities of loading on the failure modes, load carrying capacity and deformation response of the specimens. The test specimens were 2/3 scale LCFST columns; these have already been applied in

real projects in residential buildings in Cangzhou, China, as shown in Fig.2.

(a) LCFST column

(b) LCFST column frame structure

Fig.2 LCFST columns connected by steel linking plates in Cangzhou China

2.2 Specimens layout

Vertical stiffeners with a height of 100mm were welded to the top and bottom of the columns to prevent local failure at the heads of the specimens. Two steel plates with a thickness of 20mm were also welded to the tops and bottoms of the specimens to apply uniform compressive loads during testing. For the specimens tested under biaxial eccentric compression, the eccentricities were 40mm or 80mm from the centroid of the specimens along a symmetry axis, Y'-Y', as shown in Fig.3. The details of the columns are shown in Fig.4.To prevent out-of-plane buckling failure of the steel linking plates, transverse stiffeners were welded to the steel linking plates and steel tubes at a spacing of 200mm.

All specimens were divided into three groups. The first group, labeled "SR", includes the specimens differing in slenderness ratio, the second group, labeled "T", contains the specimens used to study the effects of thickness of steel linking plates, and the third group, labeled "E", consists of the specimens loaded at different eccentricities. For example, Specimen SR-13.8-1000 had a slenderness ratio λ of 13.8 and a height of 1000mm; Specimen T-3.75 means the thickness of the steel linking plates is

3.75mm; and Specimen E-40 means the eccentricity is 40mm. The test program is summarized in Table 1.

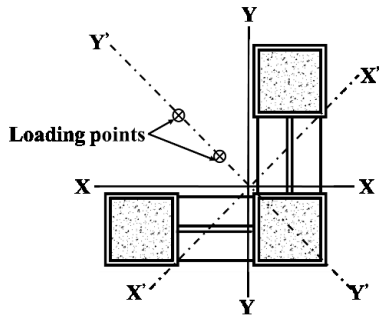

Fig.3 Arrangement of loading points for specimens under biaxial eccentric loading

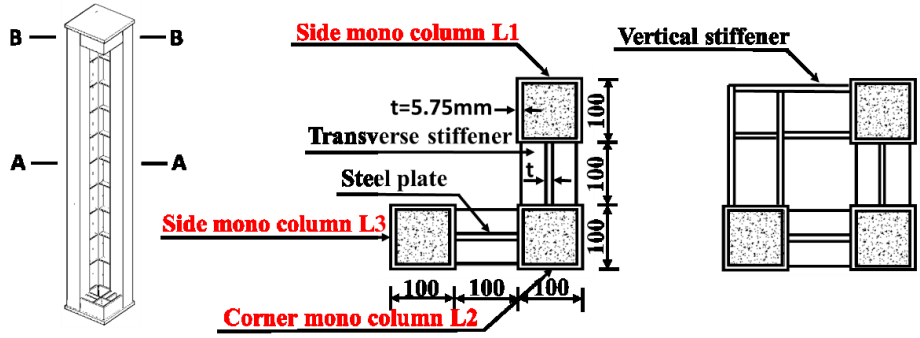

(a) Overview **(b) Cross-section A-A** **(c) Cross-section B-B**

Fig.4 Details of the test columns

Table.1 Properties of specimens

Specimen	L (mm)	λ	t (mm)	e_o (mm)
SR-13.8-1000	1000	13.8	5.75	0
SR-20.7-1500	1500	20.7	5.75	0
SR-34.5-2500	2500	34.5	5.75	0
Standard specimen	2000	27.6	5.75	0
T-3.75	2000	27.6	3.75	0
T-7.75	2000	27.6	7.75	0
E-40	2000	27.6	5.75	40
E-80	2000	27.6	5.75	80

2.3 Material properties

The material properties of the steel were determined using tensile tests on coupons taken from the steel tubes and linking plates. Concrete cube and cylinder tests were used to determine compressive strength and elastic modulus. Mechanical properties of the steel and concrete are shown in Table 2.

Table.2 Mechanical properties of steel and concrete used in the current study

Material	t (mm)	f_y (MPa)	f_u (MPa)	E_s (MPa)	ε_y ($\mu\varepsilon$)	f_c (MPa)	E_c (MPa)
Steel tube	5.75	358	439	1.51×10^5	2371	--	--
Steel plate 1	3.75	334	474	1.37×10^5	2438	--	--
Steel plate 2	5.75	319	465	1.58×10^5	2019	--	--
Steel plate 3	7.75	310	442	1.92×10^5	1740	--	--
Concrete	--	--	--	--	--	43.2	17453

2.4 Test setup and instrumentation layout

The tests were performed using a 5000 kN hydraulic compression machine, as shown in Fig. 5. To measure the longitudinal and transverse strains of the specimens, 60 strain gauges were bonded to the top, middle, and bottom of the steel tubes, except the four areas connected to the steel linking plates where strain gauges were bonded onto the mid-height of the areas. Furthermore, another two strain rosettes were bonded to the mid-heights of the steel linking plates to determine the directions of the principal strains as well as longitudinal and transverse strains under different loading conditions. Fig.6 shows the layout of strain gauges on the specimens. The lateral deflections and longitudinal displacements were measured using 16 Linear Variable Displacement Transducers (LVDTs). The arrangement of LVDTs is shown in Fig.7. Twelve LVDTs were placed at the middle and quarter parts of the specimens to measure lateral deflection. Two additional LVDTs were placed at the top, and another two at the bottom, of the specimens to measure longitudinal displacements. A load interval of

100kN was used, and each load was maintained for two minutes, the test stopped after the specimens failed.

Fig.5 Photo of test setup

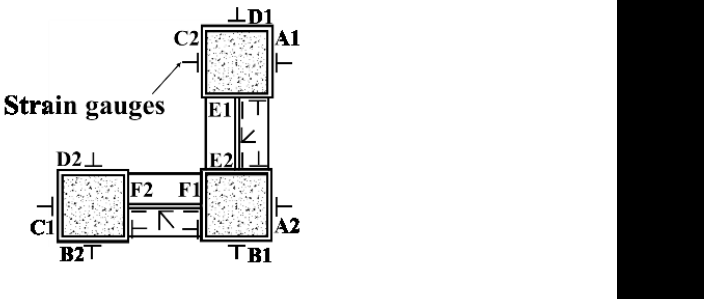

(a) Overview **(b) Right view**

Fig.6 Layout of strain gauges and strain rosettes during testing

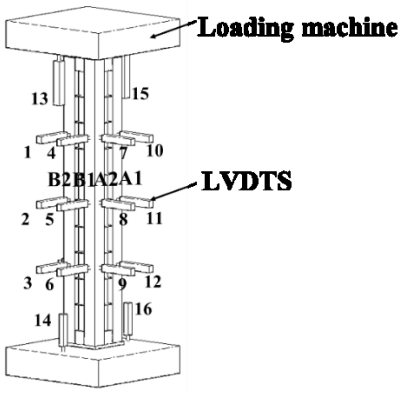

Fig.7 Schematic arrangement of LVDTs during testing

3 Experimental results and discussions

3.1 Failure mode

Fig.8 shows the failure modes of the specimens. For specimens differing in slenderness ratios, failure modes varied greatly depending on slenderness ratio. Specimen SR-13.8-1000 experienced severe local buckling combined with global bending around the X'-X' axis, which is at 45 degrees from the X-X axis (Fig.3). The deformation of Specimen SR-13.8-1000 was not obvious until peak load, when it was approaching the peak load a small sound was heard followed by dramatic deformation of the specimen. Fig.8(a) shows that severe local buckling was observed at the middle of areas C1, C2, D1, D2, the top and bottom of areasB1, A2, as well as the bottom of A1 and B2. No local buckling appeared on the areas connected to steel plates. A similar phenomenon was observed for Specimen SR-20.7-1500, however less obvious. Fig. 8(b) shows that local buckling was evident at the quarter point near the bottom of areas A1, B2, C1 and D1, and the whole column bent about the X'-X' axis. Local buckling did not appear in the areas connected to steel plates. However, different from the specimens described above, which had smaller slenderness ratios, local buckling was not observed in the standard specimen or in Specimen SR-34.5-2500, the failure modes of which were global buckling in both cases.

For specimens differing in the thickness of steel linking plates, the failure modes were also global buckling but larger out-of-plane deflection of the mono columns was observed in the specimens with smaller thickness of linking plates (as expected). Fig.8(c) shows typical failure modes of the four specimens discussed above. The failure modes of the eccentrically loaded specimens are shown in Fig.8(d). Similarly, global buckling was seen in these two specimens, and they also bent about the X'-X' axis. However, due to the large lateral deflections experienced at the middle of the

columns, local buckling appeared in the middle of the side of mono column L1 and the side of mono column L3. From the above, failure modes of LCFST columns vary along with slenderness ratio and the steel linking plates have a considerable effect on preventing the areas connected to them from local buckling.

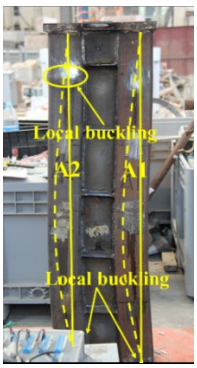

(a1) Right view

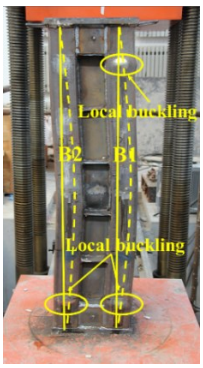

(a2) Front view

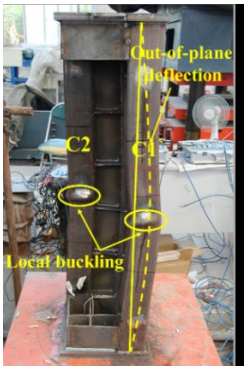

(a3) Left view

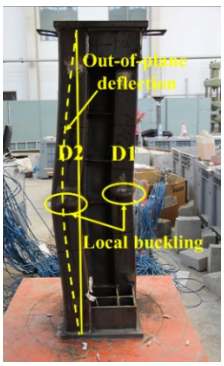

(a4) Back view

(a)Failure mode of Specimen SR-13.8-1000

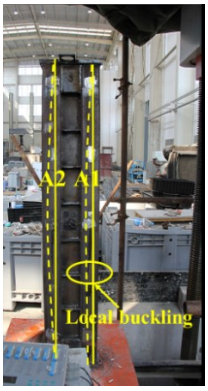

(b1) Right view

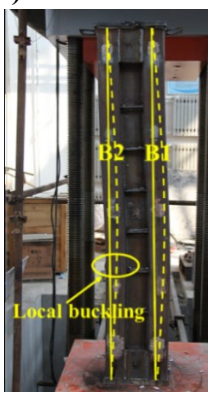

(b2) Front view

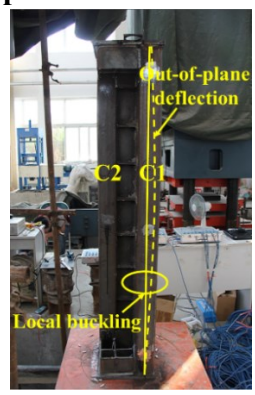

(b3) Left view

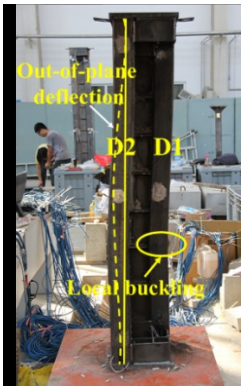

(b4) Back view

(b)Failure mode of Specimen SR-20.7-1500

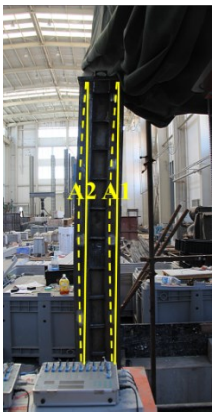

(c1) Right view

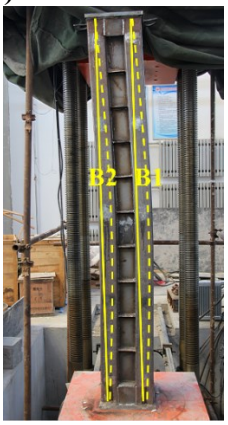

(c2) Front view

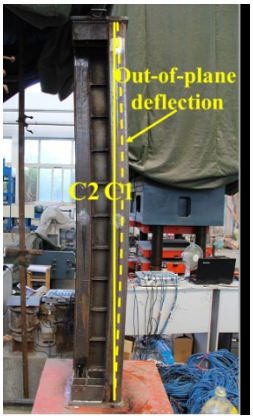

(c3) Left view

(c4) Back view

(c)Typical failure mode of specimens with the height of 2 meters or higher under axial compression

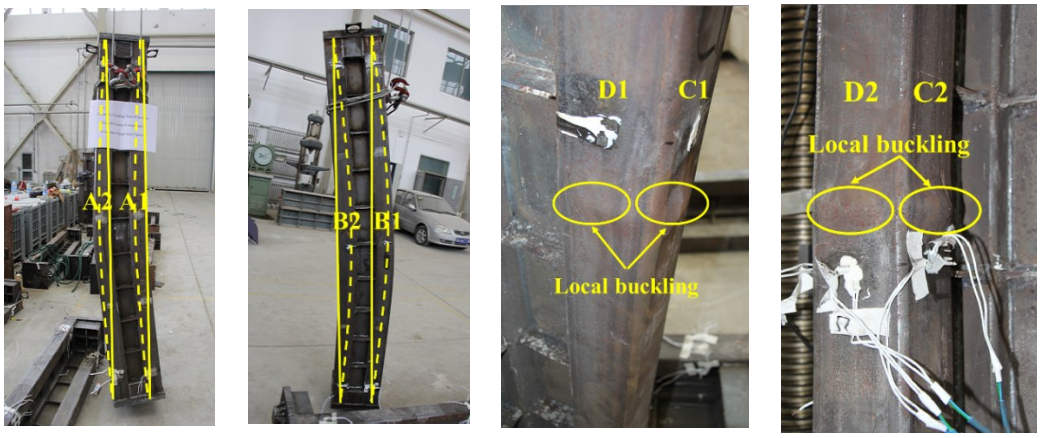

(d1) Right view (d2) Front view (d3)Mono column L3 (d4)Mono column L1

(d)Typical failure mode of eccentrically loaded specimens

Fig.8 Failure modes of the specimens

3.2 Effect of slenderness ratios

Slenderness ratio is discussed in this section along with its effect on the secant stiffness, load carrying capacity and strain distributions in LCFST columns connected by steel linking plates. Load versus longitudinal displacement relationships and load versus longitudinal stain relationships are also presented.

3.2.1 Load-longitudinal displacement relationships

Two LVDTs were set at each end to measure the vertical deformation, and the average value was considered as the displacement. The longitudinal displacement of the specimen was taken as the sum of the absolute values of the vertical displacement of the top and base plates. Fig.9 shows the axial load (N) versus longitudinal displacement curves of specimens differing by slenderness ratio. All specimens had nearly linear load-longitudinal displacement response up to the yield point. Load carrying capacity then increased at a lower rate. Fig. 9 clearly shows that a rise of slenderness ratio causes the secant stiffness to decrease, and the load carrying capacity to drop, as anticipated. Beyond the peak load, the specimens displayed a softening

branch, indicating considerable deformation ductility.

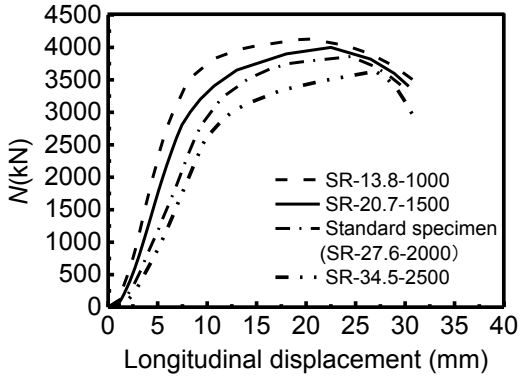

Fig.9 Axial load (*N*) versus longitudinal displacement curves for specimens with increasing slenderness ratios

3.2.2 Load-longitudinal strain relationships

The relationship between axial load and the largest longitudinal stains at the mid-height of each mono column is shown in Fig.10. Because the differences in slenderness ratios of the four specimens were not extreme, the curves are similar. Furthermore, because of the comparatively small slenderness ratios, the second-order inelastic moments had only minor effects on the specimens, resulting in compressive strains across the entire cross sections. To compare the strain distributions for side mono column L1 and side mono column L3, absolute values of the largest strains at the mid-height of side mono column L3 are shown in Fig.10(a). Some strain gauges malfunctioned at loads approaching the peak loads, so the descending branches were not recorded in some cases. Fig.10 shows that each mono column experienced an essentially linear increase in longitudinal strains during the elastic phase. The figure curves for side mono column L1 and side mono column L3 are almost symmetrical, indicating that strain distributions were similar for these mono columns. Strains of corner mono column L2 were smaller than those of the side mono columns, and the specimens with larger slenderness ratios showed smaller longitudinal strains in corner

mono column L2 under the same loads. This is likely because of bending about the X'-X' axis (see Fig.3), with corner mono column L2 located in the tensile area while the side mono columns were located in the compressive area. Corner mono column L2 was under the actions of both compressive stress caused by axial load and tensile stress caused by the second-order inelastic moment, which resulted in its smaller compressive longitudinal strains at mid-height. However, because of the small effect of second-order inelastic moments on Specimen SR-13.8-1000, the strains of the three mono columns were similar, suggesting that the axial load should have been assigned evenly to the three mono columns. According to the results obtained from the strain gauges, the largest longitudinal strains in the steel tubes of each mono column including corner mono column L2 which surpassed the yield strain of the steel tube obtained from the tensile tests when the specimens failed. This suggests that the failure mode of the four specimens discussed above was by inelastic buckling.

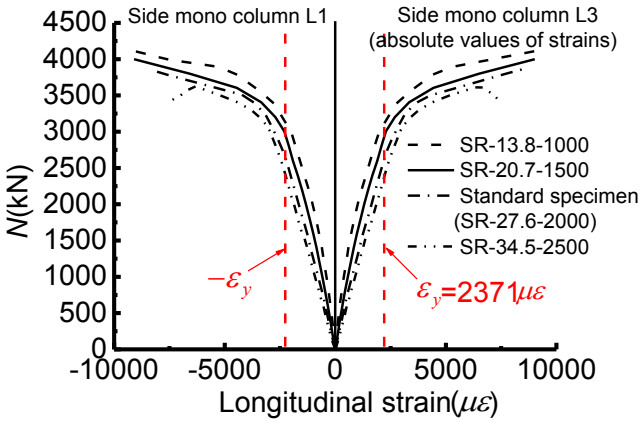

(a)Side mono column L1 and Side mono column L3

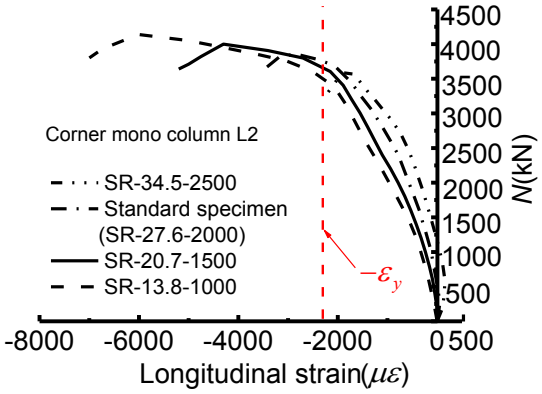

(b)Corner mono column L2

Fig.10 Axial load (*N*) versus the largest mid-height longitudinal strain curves of specimens with different slenderness ratios

3.3 Effect of thickness of steel linking plates

As the connection between the mono columns, the steel linking plates have a great influence on the response of LCFST columns. The variation of thickness of these plates is discussed with reference to its effect on the load versus deformation behavior of the columns.

3.3.1 Load-longitudinal displacement relationship

Fig.11 depicts the axial load (*N*) versus longitudinal displacement curves of the specimens differing in the thickness of steel linking plates. Increasing thickness of the steel linking plates causes a rise in the secant stiffness. Similarly, a slight rise in load carrying capacity is also apparent when increasing the plate thickness, which suggests that part of the axial loads were also taken by the steel plates (as expected). No differences were observed in the three specimens in the descending branch. The analysis above suggests that the steel linking plates have an important effect on improving the secant stiffness as well as mildly enhancing the load carrying capacity, but no obvious effect of improving ductility.

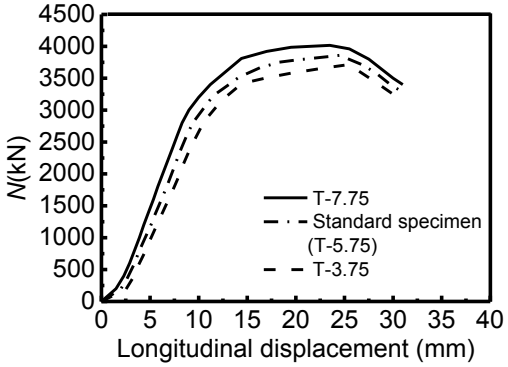

Fig.11Axial load (*N*) versus longitudinal displacement curves of specimens with different thicknesses of steel linking plates

3.3.2 Load-lateral deflection relationship

Similar to the strain distribution in the side mono columns, because of their bending about the X'-X' axis (see Fig.3), out-of-plane lateral deflections of the two side mono columns were also similar. Out-of-plane lateral deflections of Area A2 and Area B1 in the corner mono column L2 also had similar values, so the typical axial load (*N*) versus mid-height lateral deflection curves of the side mono columns, as well as the corner mono column, for Specimen T-3.75, standard specimen（T-5.75）and Specimen T-7.75 are presented in Fig.12(a) and Fig.12(b), respectively. Each mono column experienced a linear increase in lateral deflections in the elastic phase, after reaching the yield point, and lateral deflections then started to rise. The lateral stiffness of mono columns rose with increasing the steel plate thickness, thus indicating that the steel plates had a great influence on confining the lateral deflections of mono columns, which in turn delayed their out-of-plane instability. Lateral deflections of corner mono column L2 were smaller than those of side mono columns. Mid-height lateral deflections corresponding to the ultimate loads of corner mono column L2 were 9mm, 9.5mm, and 9.8mm for Specimen T-7.75, standard specimen (Specimen T-5.75) and Specimen T-3.75, respectively, while the values for side mono columns were 10.5mm,

11.2mm and 11.7mm respectively. This may result from the fact that two of the areas of the corner mono column L2 were connected to the steel linking plates and the out-of-plane deflections were thus better confined. The steel linking plates thus have a great influence on controlling the lateral deflections of mono columns, as expected.

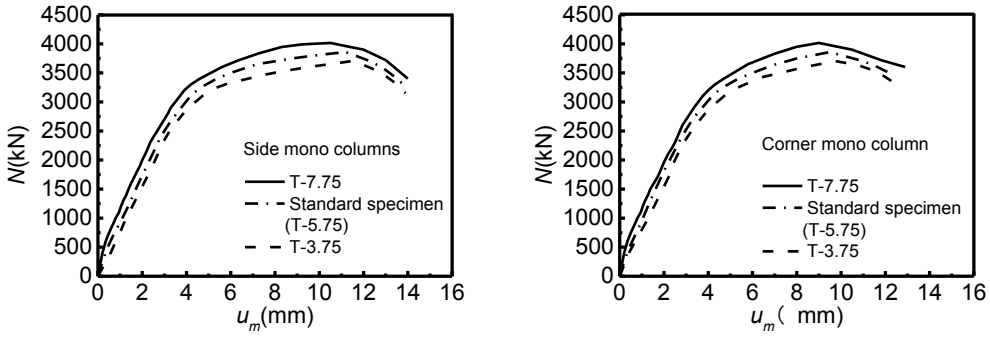

(a) Side mono columns **(b) Corner mono column**

Fig.12 Typical axial load (*N*) versus mid-height lateral deflection (u_m) curves of specimens with different thickness in steel linking plates

3.4 Effect of the eccentricity

In previous studies, the eccentric loading angle was investigated to analyze its effect on the response of LCFST columns connected by steel linking plates. It was determined that the variation of the eccentric loading angle did not strongly affect load carrying capacity. Two specimens were tested in the current study under biaxial eccentric compression, with the magnitude of the eccentricity as a variable. Eccentricities of 40mm and 80mm from the centroid of the specimens, along the symmetry axis, Y'-Y' (see Fig.3), are presented in this section.

3.4.1 Load-longitudinal displacement relationship

Fig.13 depicts the load versus longitudinal displacement relationship of the standard specimen (E-0), Specimen E-40 and Specimen E-80. It can be clearly seen that with an increase in eccentricity of loading, the secant stiffness and load carrying capacity of the specimens dropped dramatically. The ultimate loads of the standard specimen

(E-0), Specimen E-40, and Specimen E-80 were 3858kN, 2427kN and 2030kN, respectively. Thus, the ultimate load carrying capacity of Specimen E-40 and Specimen E-80 decreased 37% and 47%, respectively, compared with the standard specimen (E-0) under pure axial load. This confirms the well-known result that increasing eccentricity reduces the capacity of columns.

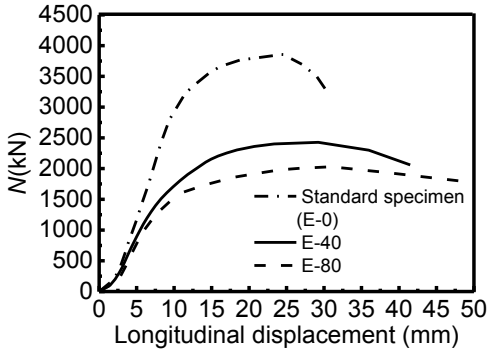

Fig.13Axial load (*N*) versus longitudinal displacement curves of specimens with different loading eccentricities

3.4.2 Load-lateral deflection relationship

Because the loading eccentricities were along the symmetry axis Y'-Y' (see Fig.3), this resulted in almost the same out-of-plane deflections of each mono column. Fig.14 shows the typical relationship between axial load and mid-height lateral deflection of the standard specimen (E-0), Specimen E-40 and Specimen E-80. Similar to the axially loaded specimens, lateral deflections of the eccentrically loaded specimens also experienced an almost linear increase before reaching the yield point. However, the lateral stiffness of the mono columns decreased more dramatically for the specimens with larger eccentricities, as expected. In addition, the confining effect of the steel linking plates on the corner mono column L2 tended to be smaller for the specimens under eccentric compression, which contributed to nearly the same out-of-plane deflections as the side mono columns. Typical lateral deflections along the column of the mono columns at different load levels for Specimen E-40 and

Specimen E-80 are shown in Fig.15; *h* denotes the distance from the bottom support. Lateral deflections of the mono columns increased slowly before the specimens reached 60 % of ultimate load, which corresponded appropriately to yielding of the material, however after reaching the yield point the lateral deflections began to rise quickly and the specimens with larger eccentricities experienced dramatic increases in lateral deflections. The curves of the mono columns were almost symmetrical about mid-span. Furthermore, although small discrepancies could be observed between the test curves and the half-sine waves, lateral deflection curves of the mono columns approximated to be half-sine waves.

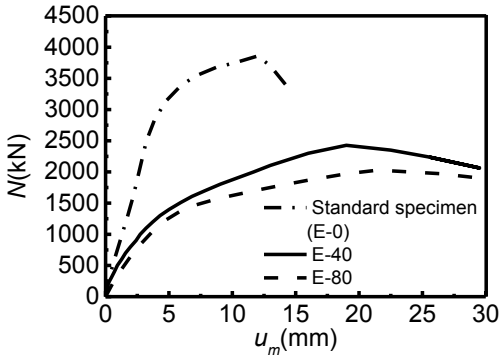

Fig.14 Typical axial load (*N*) versus mid-span lateral deflection (u_m) curves of mono columns in eccentrically loaded specimens

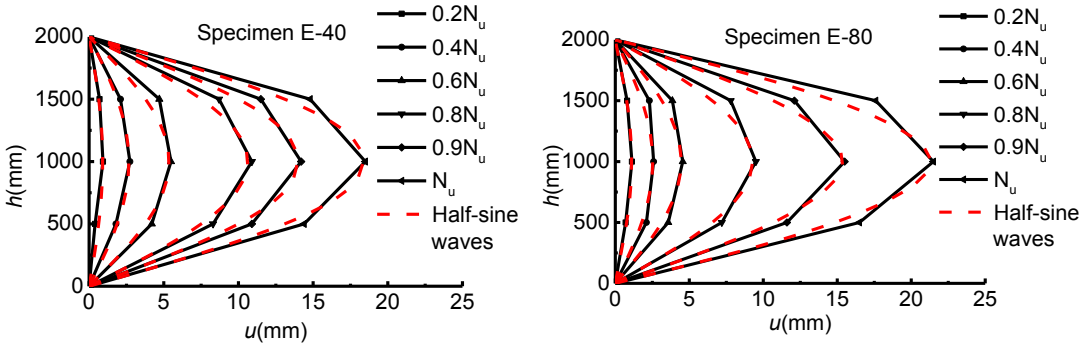

(a) Specimen E-40 **(b) Specimen E-80**

Fig.15 Typical lateral deflections (*u*) along the column of the mono columns in eccentrically loaded specimens at different load levels

3.4.3 Load-longitudinal strain relationships

The relationship between axial load and the largest longitudinal strains at the mid-height of each mono column for Specimen E-40 and Specimen E-80 is shown in Fig.16. Similar to the comparison above, absolute values of the largest compressive strains at the mid-height of side mono column L3 are shown in Fig.16 (a). Similar to the phenomenon observed in the specimens under axial load, curves of side mono column L1 and side mono column L3 are almost symmetrical for Specimen E-80. However, curves of the two side mono columns for Specimen E-40 are non-symmetrical, which may be due to initial imperfections of the specimens as well as unavoidable experimental errors. In contrast with the side mono columns, corner mono column L2 of the eccentrically loaded specimen was under a tensile state, and the largest tensile strains which appeared at the mid-height of the column are shown in Fig.16 (b). Fig.16 shows that vertical strains of all the steel tubes of the mono columns surpassed the yield strains of the steel tubes at failure, which suggests that the failure mode of these specimens was also inelastic buckling.

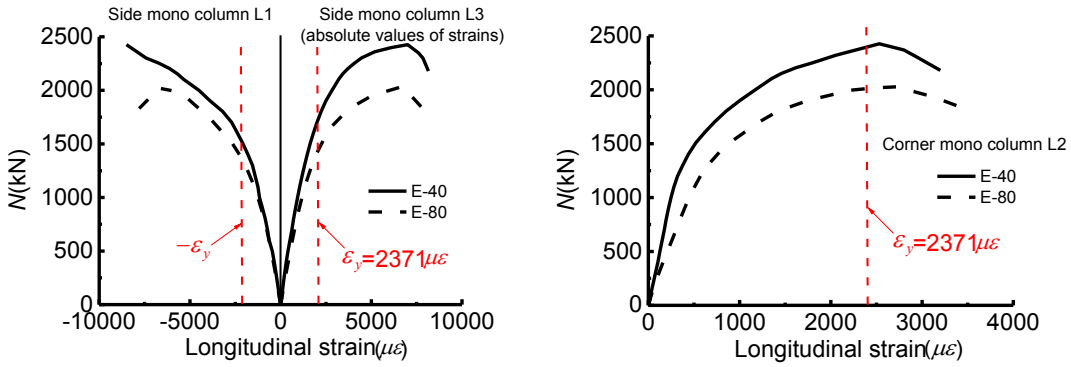

(a) Side mono columns **(b) Corner mono column**

Fig.16 Axial load (*N*) versus the largest mid-height longitudinal strain curves of specimens with different eccentricities

4 Analysis of the principal strains in the steel plates

Two strain rosettes were bonded to the two steel linking plates (see Fig. 6) to measure the principal strains during loading; these consisted of strain gauges at angles of 0^0, 45^0 and 90^0. The 0^0 strain gauges were placed in the horizontal direction. The values and directions of the principal strains of the steel linking plates were calculated using [15]:

$$\begin{cases} \varepsilon_x = \varepsilon_0 \\ \varepsilon_y = \varepsilon_{90} \\ \gamma_{xy} = 2\varepsilon_{45} - \varepsilon_0 - \varepsilon_{90} \end{cases} \tag{1}$$

$$\begin{matrix} \varepsilon_1 \\ \varepsilon_2 \end{matrix} = \frac{\varepsilon_x + \varepsilon_y}{2} \begin{matrix} + \\ - \end{matrix} \sqrt{(\frac{\varepsilon_x - \varepsilon_y}{2})^2 + (\frac{\gamma_{xy}}{2})^2} \tag{2}$$

$$tg2\theta_p = \frac{\gamma_{xy}}{\varepsilon_x - \varepsilon_y} \tag{3}$$

where γ_{xy} is the shear strain, ε_{45} is the strain obtained from the 45^0 strain gauge, ε_1 is the first principal strain, ε_2 is the second principal strain and θ_p is the angle between the direction of the first principal strain and the transverse direction.

The values of θ_p of each specimen varied irregularly with an increase of axial load, but ranged from 0^0 to 10^0, which suggests that the direction of the first principal strain ε_1 of the steel linking plates was almost horizontal and the direction of the second principal strain ε_2 thus almost vertical. Eqs. (1)-(3) suggest that the first principal strains ε_1 of each specimen were positive, indicating that they were tensile strains while the second principal strains ε_2 of each specimen were negative. In addition, the values of the second principal strains ε_2 surpassed the yield strains of the steel linking plates obtained from the tensile tests at failure, which indicates that

the steel plates contributed to the ultimate capacity. The directions of the principal strains of the steel linking plates between the two stiffeners are shown in Fig.17. Thus, the steel linking plates in the LCFST columns should be treated as thin plates, and relevant theories of thin plates can be used to design the steel linking plates so as to prevent them from local buckling before the columns failed in a global mode.

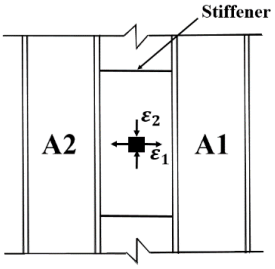

Fig.17 Directions of the principal strains in the steel linking plates between two stiffeners

5 Comparison with LCFST columns connected by lacing bars

Related research on LCFST columns connected by lacing bars was conducted [10] several years ago, and a figure of the specimen is shown in Fig.18. As described in [10], the height of the specimen is 2 meters, the size of the cross section of the specimen is absolutely the same with the standard specimen in this paper, furthermore, the mechanical properties of concrete as well as steel are very close to those of the standard specimen as well. Therefore, in this part the standard specimen is compared with the LCFST columns connected by lacing bars to reflect the advantages of LCFST columns connected by steel plates. Comparisons of the two specimens are given in Table.3. As shown in Table.3, the ultimate load of the standard specimen is larger than that of the LCFST column connected by lacing bars, which suggests that described steel plates contribute to the load carrying capacity of the column. Failure of the LCFST column connected by lacing bars under axial load was caused by the out-of-plane instability of one side mono column while the failure of the standard specimen was caused by the global buckling of the whole column which indicates that

the steel plates and the stiffeners welded to the mono columns delayed the out-of-plane instability of them and improved the integrity of the LCFST columns. The location of the largest lateral deflections of each mono column of standard specimen is at the mid-height, while that of the LCFST column connected by lacing bars varies in different mono columns which indicates that the steel plates have a higher confinement of the lateral deflections of the mono columns and they can ensure the mono columns work together. As shown in Table.3, strains of the steel plates corresponding to the ultimate loads of the columns are much larger than the yield strain while those of lacing bars are much smaller, which further verifies the hypothesis that the steel plates undertake part of the axial loads and the function of the lacing bars is just connecting the mono columns. Concluded from the comparisons above, LCFST column connected by steel plates have a much better property than the LCFST column connected by lacing bars.

Table.3 Comparisons of standard specimen and LCFST column connected by lacing bars

Specimen	Failure mode	Ultimate loads (kN)	Location of the largest lateral deflections of each mono column	Strains of steel plates or lacing bars corresponding to ultimate loads
Standard specimen	Global buckling of the whole column	3858	Mid-height	Much larger than the yield strain
LCFST column connected by lacing bars	Out-of-plane instability of one side mono column	3610	Quarter parts near the top or the bottom of the column	Smaller than the yield strain

Fig.18 LCFST column connected by lacing bars

6 Calculating the ultimate capacity of LCFST columns connected by steel linking plates

Predictive formulas for the ultimate loads of LCFST columns connected by steel linking plates are proposed based on a modification of American national standard for structural steel buildings ANSI/AISC 360-05[14] for determining the ultimate loads of steel laced columns, as well as concrete-filled steel tubular columns. Values of the ultimate loads obtained from the predictive formulae are compared with the experimental results in this section.

According to ANSI/AISC 360-05 [14], design formulae for laced columns are the same as those for mono columns after modification of the slenderness ratio. Modification of the slenderness ratio for intermediate connectors that are welded is determined as follows:

$$(\frac{KL}{r})_m = \sqrt{(\frac{KL}{r})_o^2 + 0.82\frac{\alpha^2}{(1+\alpha^2)}(\frac{a}{r_{ib}})^2} \quad (4)$$

Where $(\frac{KL}{r})_m$ is the modified column slenderness for laced columns, $(\frac{KL}{r})_o$ is the column slenderness of laced column acting as a unit, in the buckling direction being considered, a is the distance between connectors, for columns connected by lacing bars this is the distance between the centroidal axis of the adjacent transverse lacing

bars, and for those connected by batten plates it is the distance between the centroidal axis of the adjacent batten plates. r_{ib} is the radius of gyration of each individual component relative to its centroidal axis, parallel to member axis of buckling, and α is the separation ratio.

Modification of the slenderness ratios for laced columns are used to involve the effect of the shear deformation of the connectors on the ultimate capacity of the columns. However, since steel linking plates welded to the mono columns distributed along the height of the specimens, along with transverse stiffeners welded to the steel linking plates which have a great confinement on the deformation of steel linking plates, thus shear deformation of the steel linking plates is so small that its effect can be neglected in calculating the response of the columns. This idea can also be verified by considering Eqn. (4) with the distance between connectors assumed as zero, so $(\frac{KL}{r})_m$ is equal to $(\frac{KL}{r})_o$.

As specified in ANSI/AISC 360-05, the design compressive strength of axially-loaded concrete-filled steel tubular columns should be determined as:

(a) When $P_e > 0.44P_o$,

$$P_n = P_o[0.658^{(\frac{P_o}{P_e})}] \tag{5}$$

(b) When $P_e < 0.44P_o$,

$$P_n = 0.877P_e \tag{6}$$

$$P_o = A_s F_y + A_{sr} F_{yr} + 0.85A_c f_c^{'} \tag{7}$$

$$P_e = \pi^2 (EI_{eff}) / (KL)^2 \tag{8}$$

$$EI_{eff} = E_s I_s + E_s I_{sr} + C_3 E_c I_c \tag{9}$$

$$C_3 = 0.6 + 0.2(\frac{A_s}{A_c + A_s}) \leq 0.9 \quad (10)$$

Where K is the effective length factor. Because the bottom plate of the testing machine used herein can rotate while the top plate is rotationally fixed, the end conditions of the specimens can be assumed as: 1) for specimens under axial compression, rotation is free and translation is fixed for bottom end while rotation is fixed and translation is fixed for top end, so K=0.7; 2) for specimens under eccentric compression, steel cubes were welded to both ends of the specimens to apply eccentric loads and they can rotate throughout the loading process, so rotation is free and translation is fixed for both ends of the specimens, thus K=1.0. P_o is the nominal axial compressive strength without consideration of length effect, P_n is nominal axial strength, P_e is elastic critical buckling load, EI_{eff} is effective stiffness of composite section, A_s, A_{sr}, and A_c are the cross-sectional areas of the steel tube, reinforcing bars, and concrete respectively. E_s, E_c are the modulus of elasticity of the steel and concrete, respectively. I_s, I_{sr}, and I_c are the moments of inertia of the steel tube, reinforcing bars, and concrete section, respectively.

To calculate the ultimate capacity of LCFST columns connected by steel linking plates, the steel linking plates' contributions to load capacity should be included when calculating P_o, so that P_o is equal to $3A_sF_y + 2A_{sp}F_{yp} + 0.85 \times 3A_cf_c^{'}$, where A_{sp} and F_{yp} are the cross-sectional areas and yield strengths of the steel plates. Calculated results obtained from the formulae above are given in Table.4.

For the eccentrically loaded specimens, no specific provisions are available for concrete-filled steel tubular laced columns in ANSI/AISC 360-05. Chen et al. [16] suggested that the effects of slenderness and eccentricities on the ultimate carrying

capacity of concrete-filled steel tubular laced columns were independent after some experimental and theoretical investigation, and a coefficient to account for different eccentricities was proposed. Relevant provisions are available in the Chinese national technical code for concrete-filled steel tubular structures GB 50936-2014[17]. As stated in GB 50936-2014, the formulae for the coefficient with the consideration of eccentricity are:

(a) When $e_0 / a_c \le 2$,

$$\varphi_e = \frac{1}{1 + e_0 / a_t} \qquad (11)$$

(b) when $e_0 / a_c > 2$,

$$\varphi_e = \frac{1}{3(e_0 / a_c - 1)} \qquad (12)$$

$$e_0 = M_2 / N \qquad (13)$$

$$a_t = \frac{N_0^c}{N_0^c + N_0^t} \times h \qquad (14)$$

$$a_c = \frac{N_0^t}{N_0^c + N_0^t} \times h \qquad (15)$$

where φ_e is the coefficient related to eccentricity, e_0 is the eccentricity of loading, a_c is the distance between the centroid of the compressive mono columns and the centroid of the whole column under pure bending, a_t is the distance between the centroid of the tensile mono columns and the centroid of the whole column under pure bending, h is the distance between the centroid of the tensile mono columns and the centroid of the compressive mono columns under pure bending. N_0^t is the sum of the compressive ultimate loads of the mono columns in the tensile region without consideration of length effects under pure bending, N_0^c is the sum of the compressive

ultimate loads of the mono columns in the compressive region without consideration of length effects under pure bending.

A schematic description of the characters above is shown in Fig.19. The coefficient related to eccentricity φ_e is used to calculate the ultimate capacities of the eccentrically loaded specimens in the current study; these are also presented in Table4. Calculated results agree reasonably well with experimental values. The hypotheses of neglecting the effect of the shear deformation of the steel linking plates, as well as including the steel linking plates' moderate contributions to P_o, are therefore both reasonable, and the predictive formulae for the ultimate loads of LCFST columns connected by steel linking plates based on a modification of the ANSI/AISC 360-05 equations appear to be suitable designing such columns.

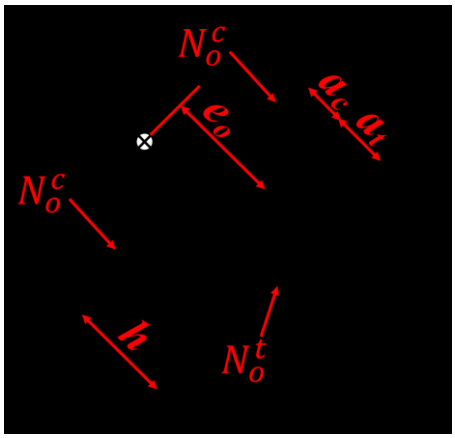

Fig.19 Schematic description of the characters used in the equations of the current section

Table.4 Comparisons of the predicted ultimate load capacities and the experimental results

Specimen	N_u	$N_{u\exp}$	$N_{u\exp} / N_u$
SR-13.8-1000	4040	4138	1.024
SR-20.7-1500	3980	4000	1.005
SR-34.5-2500	3800	3632	0.956

Standard specimen	3900	3858	0.989
T-3.75	3790	3705	0.978
T-7.75	4000	4015	1.004
E-40	2560	2427	0.948
E-80	2020	2030	1.005
Average			0.989
Standard deviation			0.025

7 Conclusions

This paper has presented an experimental investigation into the fundamental structural behavior of L-shaped columns composed of concrete-filled steel tubes (LCFST columns) connected by steel linking plates. A total of 8 large-scale specimens were tested to study the effects of slenderness ratio, the thickness of the steel linking plates, and the eccentricity of loading. The following conclusions can be drawn based on the research work reported in the paper:

(1) Failure modes of LCFST columns connected by steel linking plates varied with a change of slenderness ratio. Specimens with small slenderness ratios displayed local buckling in different parts of mono columns. Steel linking plates and the transverse stiffeners had a considerable influence on preventing local buckling of the tube walls.

(2) The ultimate loads of the specimens were consistent with the anticipated trends that with the increase of slenderness ratios or loading eccentricities, the resistances of the columns decreased. Ultimate loads of the specimens with slenderness ratios of 13.8, 20.7, 27.6, 34.5 are 4138kN, 4000kN, 3858kN and 3632kN respectively. Also ultimate loads of the specimens with eccentricities of 0mm, 40mm, 80mm are 3858kN, 2427kN and 2030kN respectively.

(3) The stiffness of the columns, as well as the lateral stiffness of the mono columns, was augmented with an increase of thickness of the steel linking plate. However,

changing the thickness of steel plates did not have a noticeable effect on the ductility of the columns.

(4) Compared with LCFST columns connected by lacing bars, LCFST columns connected by steel linking plates have higher load carrying capacity as well as better integrity. Each mono column can work together under the connection of the steel linking plate and the functions of the steel linking plates are not only connecting the mono columns but also undertaking part of the axial loads.

(5) Calculated values of the ultimate loads of the specimens obtained from the predictive formulas presented herein agree reasonably well with the test results. Neglecting the effect of the shear deformation of steel plates, as well as including the steel linking plates' moderate contributions to P_o is reasonable. The predictive formulas for the ultimate loads of LCFST columns connected by steel linking plates based on the modification of ANSI/AISC 360-05 appear to be suitable.

Nomenclature

a Distance between connectors

For columns connected by lacing bars it is the distance between the centroidal axis of the adjacent transverse lacing bars

For columns connected by batten plates it is the distance between the centroidal axis of the adjacent batten plates

a_c Distance between the centroid of the compressive mono columns and the centroid of the whole column under pure bending

a_t Distance between the centroid of the tensile mono columns and the centroid of the whole column under pure bending

A_c Cross- sectional areas of concrete

A_s Cross- sectional areas of steel tube

A_{sr} Cross- sectional areas of reinforcing bars

A_{sp} Cross-sectional area of steel plate

e_o Eccentricity of loading

E_c Elastic modulus of concrete

E_s Elastic modulus of steel

EI_{eff} Effective stiffness of composite section

f_c Compressive strength of concrete

f_u Ultimate strength of steel

f_y Yield strength of steel

F_{yp} Yield strength of steel plates

h Distance between the centroid of the tensile mono columns and the centroid of the compressive mono columns under pure bending

I_c Moment of inertia of concrete

I_s Moment of inertia of steel tube

I_{sr} Moment of inertia of reinforcing bars

$(\frac{KL}{r})_m$ Modified column slenderness of laced columns

$(\frac{KL}{r})_o$ Column slenderness of laced column acting as a unit in the buckling direction being considered

L Height of the specimen

N Axial load

N_o^c Sum of the compressive ultimate loads of the mono columns in the compressive region without consideration of length effect under pure bending

N_o^t Sum of the compressive ultimate loads of the mono columns in the tensile region without consideration of length effect under pure bending

N_u Calculated ultimate load of the specimen

$N_{u\exp}$ Experimental ultimate load of the specimen

P_e Elastic critical buckling load

P_n Nominal axial strength

P_o Nominal axial compressive strength without consideration of length effect

r_{ib} Radius of gyration of individual component relative to its centroidal axis parallel to member axis of buckling

t Thickness of steel

u Lateral deflection of mono column

u_m Mid-span lateral deflection of mono column

α Separation ratio

γ_{xy} Shear strain of steel plate

ε_1 ε_2 Principal strain of steel plate

ε_x Horizontal strain of steel plate

ε_y Vertical strain of steel plate

ε_0 Strain obtained from the 0^0 strain gauge

ε_{45} Strain obtained from the 45^0 strain gauge

ε_{90} Strain obtained from the 90^0 strain gauge

θ_p Angle between direction of the first principal strain and transverse direction

λ Slenderness ratio of the specimen

φ_e Coefficient related to eccentricities

Acknowledgements

The research work reported herein was sponsored by the National Natural Science Foundation of China (Grant no. NSFC51308387). The financial support is highly appreciated. Bisby is a member of the Edinburgh Research Partnership in Engineering (ERPE), and wished to acknowledge to ERPE's support and that of the School of Engineering at the University of Edinburgh.

References

[1] Ramamurthy LN, Hafeez KTA. L-shaped column design for biaxial eccentricity. Journal of Structural Engineering 1983; 109(8):1903-1917.

[2] Joaquin M. Design aids for L-shaped reinforced concrete columns. ACI Structural Journal 1979; 76(49):1197-1216.

[3] Dundar C, Sahin B. Arbitrarily shaped reinforced concrete members subjected to biaxial bending and axial load. Computers & Structures 1993; 49(4):643-662.

[4] Tokgoz C, Dundar C. Tests of eccentrically loaded L-shaped section steel fibre high strength reinforced concrete and composite columns. Engineering structures 2012; 38:134-141.

[5] Yang YL, Yang H, Zhang SM. Compressive behavior of T-shaped concrete filled steel tubular columns. International Journal of Steel Structures 2010; 10(4): 419-430.

[6] Shen ZY, Lei M, Li YQ, Lin ZY, Luo JH. Experimental study on seismic behavior of concrete-filled L-shaped steel tube columns. Advances in Structural Engineering 2013; 16(7):1235-1247.

[7] Chen ZH, Li Z, Rong B, Liu X. Experiment of axial compression bearing capacity for crisscross section special-shaped column composed of concrete-filled square steel tubes. Journal of TianJin University 2006; 39(11): 1275-1282 (in Chinese).

[8] Chen ZH, Rong B, Fafitis A. Axial compression stability of a crisscross section column composed of concrete-filled square steel tubes. Journal of Mechanics of Materials and Structures 2009; 4(10):1787-1799.

[9] Rong B. Theoretical analysis and experimental study on special-shaped column composed of concrete-filled square steel tubes. Tianjin: Tianjin University Press; 2008 (in Chinese).

[10] Zhou T, Xu MY, Wang XD, Chen ZH, Qin Y. Experimental study and parameter analysis of L-shaped composite column under axial loading. International Journal of Steel Structures 2015; 15(4) : 797-807.

[11] Zhou T, Chen ZH, Liu HB. Seismic behavior of special shaped column composed of concrete filled steel tubes. Journal of Constructional Steel Research 2012; 75:131-141.

[12] Zhou T, Li XF, Xu MY. Heat transfer property of special-shaped column composed of concrete-filled steel tubes. Journal of Tianjin University Science and Technology 2015; 48:74-80 (in Chinese).

[13] Zhou T, Jia YM, Xu MY, Wang XD, Chen ZH. Experimental study on the seismic performance of L-shaped column composed of concrete-filled steel tubes frame structures. Journal of Constructional Steel Research 2015；114:77-88.

[14] ANSI/AISC 360-05: Specification for Structural Steel Buildings, American Institute of Steel Construction, 2005.

[15] Li ZX. Theory and technique of engineering structure experiments. Tianjin: Tianjin University Press; 2004 (in Chinese).

[16] Chen BC, Ou ZQ. Calculation method for the ultimate load carrying capacity of concrete-filled steel tubular lattice columns. China Civil Engineering Journal 2008; 41(1):55-63 (in Chinese).

[17] GB 50936-2014: Chinese National Technical Code for Concrete-filled Steel Tubular Structures, Chinese Institute of Housing and Urban-rural Development, 2014 (in Chinese).